Solar magnetic flux tube simulations with time-dependent ionization

D. E. Fawzy[1]⋆, M. Cuntz[2] and W. Rammacher[3]

[1] *Faculty of Engineering and Computer Sciences, Izmir University of Economics, Izmir 35330, Turkey*
[2] *Department of Physics, University of Texas at Arlington, Box 19059, Arlington, TX 76019, USA*
[3] *Kiepenheuer-Institut für Sonnenphysik, Schöneckstr. 6, 79104 Freiburg, Germany*

ABSTRACT

In the present work we expand the study of time-dependent ionization previously identified to be of pivotal importance for acoustic waves in solar magnetic flux tube simulations. We focus on longitudinal tube waves (LTW) known to be an important heating agent of solar magnetic regions. Our models also consider new results of wave energy generation as well as an updated determination of the mixing length of convection now identified as 1.8 scale heights in the upper solar convective layers. We present 1-D wave simulations for the solar chromosphere by studying tubes of different spreading as function of height aimed at representing tubes in environments of different magnetic filling factors. Multi-level radiative transfer has been applied to correctly represent the total chromospheric emission function. The effects of time-dependent ionization are significant in all models studied. They are most pronounced behind strong shocks and in low density regions, i.e., the middle and high chromosphere. Concerning our models of different tube spreading, we attained pronounced differences between the various types of models, which were largely initiated by different degrees of dilution of the wave energy flux as well as the density structure partially shaped by strong shocks, if existing. Models showing a quasi-steady rise of temperature with height are obtained via monochromatic waves akin to previous acoustic simulations. However, longitudinal flux tube waves are identified as insufficient to heat the solar transition region and corona in agreement with previous studies.

Key words: hydrodynamics — MHD — shock waves — waves — Sun: chromosphere — Sun: surface magnetism

1 INTRODUCTION

The outer atmospheric activity of the Sun as well as other late-type stars is largely determined by the structure and time evolution of photospheric magnetic fields. These fields extend into the stellar outer atmosphere, where they cause nonradiative energy to be deposited (e.g., Anderson & Athay, 1989; Linsky, 1991; Schrijver, 2001; Bogdan et al., 2003; Roberts, 2004; Ulmschneider & Musielak, 2004; Musielak, 2004). This energy is distributed over the chromosphere, transition region, and corona; it is also considered pivotal for the heating and acceleration of solar and stellar winds. For new observations and simulations of the relative importance of acoustic and magnetic energy deposition in the solar chromosphere, see, e.g.,

Fossum & Carlsson (2005), Cuntz, Rammacher & Musielak (2007), Kalkofen (2007), and Bello González et al. (2009). Recent joint observational and theoretical studies aimed at elucidating the significance of wave heating in the solar photosphere and lower chromosphere were given by Beck & Rammacher (2010), Beck, Rezaei & Puschmann (2012), and Wedemeyer-Böhm et al. (2012). The latter study investigates the channeling of magnetic energy through the solar chromosphere into the corona, thus resembling super-tornadoes under solar conditions. Notable reviews aimed at solar chromospheric and coronal heating were given by Narain & Ulmschneider (1996), Klimchuk (2006), and Erdélyi & Ballai (2007).

Magnetic flux tubes are an important feature of the solar surface structure (e.g., Spruit & Roberts, 1983; Solanki, 1996; Schrijver & Zwaan, 2000). Both observational and theoretical studies showed that they are carriers of longitudinal tube waves (e.g., Herbold et al., 1985; Solanki & Roberts, 1992; Hasan & van Ballegooijen,

⋆ E-mail: diaa.gadelmavla@izmirekonomi.edu.tr   (DEF);
cuntz@uta.edu (MC); wrammacher@online.de (WR)

2008), which give rise to considerable temperature increases as function of height as revealed by chromospheric spectral features. In this paper, we continue to pursue our previous line of research focused on the generation of different types of waves (e.g., Narain & Ulmschneider, 1996), effects of the propagation and dissipation of waves (e.g., Herbold et al., 1985; Fawzy, Ulmschneider & Cuntz, 1998; Cuntz et al., 1999), and the emergence of chromospheric emission (e.g., Cuntz et al., 1999; Fawzy et al., 2002; Rammacher & Cuntz, 2003). However, in accord with previous simulations of acoustic waves (e.g., Carlsson & Stein, 1992, 1995; Rammacher & Ulmschneider, 2003; Rammacher & Cuntz, 2005b; Cuntz et al., 2007), the described longitudinal wave simulations will also employ time-dependent (i.e., non-instantaneous) ionization. The geometrical and thermodynamic properties of the tube atmospheres are expected to also impact the dissipation of the wave energy as well as the so-called energy velocity as recently pointed out by Worrall (2012). Time-dependent ionization entails that, e.g., behind strong shocks the long timescales of hydrogen ionization / recombination initially prevent the dissipated energy to be converted into ionization energy, thus leading to strong temerature spikes as well as a variety of other dynamic phenomena.

There exists a great motivation to revisit the dissipation of acoustic and magnetic waves in the solar chromosphere, which is the new determination of the mixing length near the top of the solar convective zones. Stein et al. (2009a,b) who provided new state-of-the-art simulations of the solar convection zone on the scale of supergranules, extending 10% of its depth but half of its pressure scale height, deduced a mass mixing length of $\alpha_{\mathrm{ML}} = 1.8$, thus superseding the previous results of 1.5 or 2.0 (Steffen, 1993; Trampedach et al., 1997), which were widely used in previous solar heating computations.

In our study we will also consider the relevance of tube spreading, i.e., different tube opening radii, for the energetics and thermodynamics of the magnetically heated solar chromospheric structure. Early results based on adiabatic longitudinal waves without the consideration of time-dependent ionization have been given by Fawzy et al. (1998). They found that the tube shape is of critical importance for the heating of flux tubes. In fact, tubes of wide opening radii show little heating, whereas constant cross section tubes show very large heating at all heights. Previous simulations of longitudinal waves for solar coronal tube structure have been given by, e.g., Ofman, Nakariakov & DeForest (1999), Ofman, Nakariakov & Sehgal (2000), and Cuntz & Suess (2004). These results further highlight the importance of tube spreading with respect to the shock wave amplitude and time-dependent and height-dependent heating rate. Concerning the formation of Ca II and Mg II emission, we will consider a two-component (magnetic and acoustic) model of the solar chromosphere with heating by longitudinal tube waves inside the flux tubes and heating by acoustic waves outside the flux tubes.

The governing equations as well as the methods of our study, including the computation of the initial flux tube models, are discussed in Sect. 2. In Sect. 3, we describe the results of our longtitudinal wave simulations for solar flux tube models with different tube spreadings; the latter correspond to different magnetic filling factors. The focus of these studies concerns the effects of time-dependent ionization. Our summary and conclusions are given in Sect. 4.

2   METHODS

2.1   Theoretical approach

In the following, we summarize some of the key equations with focus on longitudinal MHD tube waves propagating along the vertically directed magnetic flux tubes. Following previous work by, e.g., Herbold et al. (1985), the equations to be solved in the Euler frame for continuous 1-D flows are given as

$$\frac{\partial \rho A}{\partial t} + \frac{\partial \rho u A}{\partial x} = 0 , \qquad (1)$$

$$\frac{\partial u}{\partial t} + u\frac{\partial u}{\partial x} + \frac{1}{\rho}\frac{\partial p}{\partial x} + g(x) = 0 , \qquad (2)$$

$$\frac{\partial S}{\partial t} + u\frac{\partial S}{\partial x} = \left.\frac{dS}{dt}\right|_{\mathrm{rad}} , \qquad (3)$$

$$\Phi = A \cdot B = \mathrm{const} , \qquad (4)$$

$$\frac{B^2}{8\pi} + p = p_e = \epsilon p . \qquad (5)$$

Here all variables have their usual meaning. Note that p and p_e are the gas pressures inside and outside the tube, respectively, B is the magnetic field strength, and $\epsilon = p_e : p$ denotes the pressure ratio between outside and inside of the tube. Furthermore, the cross section A is time-dependent owing to the distensibility of the tube (e.g., Lighthill, 1978). Moreover, Eqs. (4) and (5) represent the conservation of the magnetic flux Φ and the horizontal pressure balance between inside and outside the tube. All quantities are both functions of height x and time t; strictly speaking, this also applies to p_e where we however assume $p_e = p_e(x)$ in accord to previous studies (e.g., Herbold et al., 1985; Cuntz et al., 1999), as we do not consider the effects of the time-dependency of the outside medium toward the tube.

Similar to the case of acoustic waves (e.g., Ulmschneider et al., 1977; Cuntz & Ulmschneider, 1988), the system of equations can be transformed into its characteristic form as pursued in detail by Rammacher & Ulmschneider (2003). A key equation concerns the behaviour of the thermodynamic variables along the C^0 characteristics with the relevant compatibility relation given as

$$dS = \left.\frac{dS}{dt}\right|_{\mathrm{rad}} dt , \qquad (6)$$

which can also be written as

$$dT - \left(\frac{\partial T}{\partial p}\right)_S dp - \left(\frac{\partial T}{\partial S}\right)_p \left.\frac{dS}{dt}\right|_{\mathrm{rad}} dt = 0 . \qquad (7)$$

Note that, e.g., $(\partial T/\partial p)_S$ and $(\partial T/\partial S)_p$ constitute well-known thermodynamic relationships (e.g., Mihalas & Mihalas, 1984); they need to be solved numerically if deviations from the thermodynamic equilibrium, as in case of our study, are considered.

The rate equations for the general case of flows have been discussed in detail by, e.g., Mihalas & Mihalas (1984) and have been implemented into actual OHD/MHD codes

by Carlsson & Stein (2002), Rammacher & Ulmschneider (2003), among others. Assuming a simplified hydrogen atom of $N = 3$ levels, namely two bound levels plus the continuum level, while considering radiative processes R and collisional processes C, the population density of level i can be obtained through solving

$$\frac{\partial n_i}{\partial t} + \frac{\partial n_i u}{\partial x} = \sum_{j=1 \,\wedge\, j\neq i}^{N} (n_j P_{ji} - n_i P_{ij}) \; , \qquad (8)$$

where P_{lk} denotes the rate of transitions (per cm^3 and s) taking place from level l to level k and $P_{lk} = R_{lk} + C_{lk}$. This equation represents the conservation equation for the particle number density n_i; however, it also takes into account the generation and destruction of n_i caused by transitions from and to other levels[1]. The LHS of Eq. (8) would be zero if the particles of species i were conserved; in this case, Eq. (8) would represent the standard continuity equation for particles of species i.

If time-dependent (i.e., noninstantaneous) ionization processes are considered, the change in the population density for the continuum level is given as

$$\frac{dn_c}{dt} = \sum_{i=1}^{N-1} n_i (R_{ic} + C_{ic}) - n_c \sum_{i=1}^{N-1} (R_{ci} + C_{ci}) - n_c W \quad (9)$$

(Rammacher & Ulmschneider, 2003); the latter also requires the time-dependent solution of the advection term given as

$$W = \rho \left(\frac{\partial T}{\partial p} \right)_S \frac{dS}{dt}\bigg|_{\mathrm{rad}} - \frac{1}{\rho c_S^2} \frac{dp}{dt} \; , \qquad (10)$$

where c_S denotes the adiabatic sound speed given as

$$c_S = \left[\left(\frac{\partial p}{\partial \rho} \right)_S \right]^{1/2} = \left[\left(\frac{\partial \rho}{\partial p} \right)_T + \left(\frac{\partial \rho}{\partial T} \right)_p \left(\frac{\partial T}{\partial p} \right)_S \right]^{-1/2} . (11)$$

The number density of the hydrogen continuum population is closely related to the electron density n_e, which is of critical importance for the manifestation of the chromospheric radiative emission function (e.g., Vernazza, Avrett & Loeser, 1981; Avrett, 1985). Other equations concern the conservation of the total number of hydrogen particles n_{tot}, given as

$$\frac{1 + Z_{\mathrm{el}}}{X_{\mathrm{el}}} \sum_{i=1}^{N-1} n_i \; + \; \left(1 + \frac{1 + Z_{\mathrm{el}}}{X_{\mathrm{el}}}\right) \; n_c \; = \; \frac{p}{kT} \; = \; n_{\mathrm{tot}} \; , (12)$$

and the conservation of electrons, given as

$$n_e \; = \; \left(1 + \frac{Z_{\mathrm{el}}}{X_{\mathrm{el}}}\right) \; n_c \; + \; \frac{Z_{\mathrm{el}}}{X_{\mathrm{el}}} \sum_{i=1}^{N-1} n_i \; , \qquad (13)$$

where X_{el} and Z_{el} denote the element abundances of hydrogen and the metals, respectively. Note that p is the gas

---

[1] Equation (8) is in line with the earlier work by Rammacher & Ulmschneider (2003). In Carlsson & Stein (2002) based on a 6-level atom it was shown that hydrogen ionization goes with collisional excitation to $n = 2$, then with radiative ionization to the continuum, a pattern broadly consistent with the present study. On the other hand, Carlsson & Stein (2002) found that recombination transitions occur by going from the continuum level to excited levels with $n > 2$, which is not possible in the 3-level atom selected.

pressure, T is the temperature, and k is Boltzmann's constant.

2.2   Comments on the (magneto-)hydrodynamic computer code

The treatment of acoustic and longitudinal flux tube waves concerning solar and stellar chromospheric models is pursued based on the code by Rammacher & Ulmschneider (2003) and subsequent augmentations by Rammacher & Cuntz (2005b). This code is suitable for the simulation of one-dimensional wave propagation and dissipation and, moreover, also allows the treatment of time-dependent (i.e., non-instantaneous) ionization processes for hydrogen and other elements by obtaining solutions of the time-dependent statistical rate equations (see also Carlsson & Stein 1992, 1995). Additional features of the code encompass the evaluation of the radiative losses (and gains) by also taking into account departures from local thermodynamic equilibrium (NLTE). Shocks are treated as discontinuities based on adequate solutions of the Rankine-Hugoniot relations; see, e.g., previous work by Nieuwenhuijzen et al. (1993) for a quasi-analytic method for the computation of the thermodynamic relationships across shocks in the presence of radiative and ionization processes.

The method of Rammacher & Ulmschneider (2003) is suitable for the treatment of both monochromatic and spectral waves. In the framework of our models, time-dependent ionization is considered with respect to hydrogen as well as magnesium and calcium. Regarding the chromospheric emission losses, we provide a detailed treatment of the Ca II K and Mg II k lines; the total chromospheric emission losses are obtained via appropriate scaling; see, e.g., Cuntz et al. (1999) for previous applications of this approach. The scaling factors have been determined by inspecting representative solutions of the wave models and by applying multi-level radiative transfer computations with MULTI (see Rammacher et al. 2005). Radiative transfer in the continuum, notable H$^-$, is pursued following the method of Schmitz, Ulmschneider & Kalkofen (1985). Another important aspect of our calculations is the implementation of boundary conditions. At the top boundary, a transmitting boundary condition is used, whereas at the bottom boundary, the injection of the magnetic or acoustic wave energy flux is simulated via a piston-type boundary condition; the latter is suitable for monochromatic waves as well as acoustic and LTW frequency spectra; see Rammacher & Ulmschneider (2003) and references therein for details.

2.3   Wave energy fluxes and wave energy spectra

The wave energy fluxes and wave energy spectra are calculated following the approach by Musielak et al. (1994) and Ulmschneider, Theurer & Musielak (1996); see also Fawzy & Cuntz (2011) for updated results pertaining to a grid of models for a set of main-sequence stars including the Sun. These types of models incorporate a detailed description of the spatial and temporal spectrum of the turbulent flow to obtain adequate results for the frequency integrated

Table 1. Acoustic and LTW energy generation.

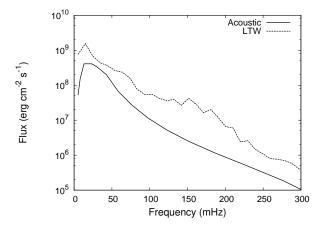| α_{ML}	Acoustic		LTW	
... ...	u_t (cm s^{-1})	F_{M} (ergs cm^{-2} s^{-1})	u_t (cm s^{-1})	F_{M} (ergs cm^{-2} s^{-1})
1.5	5.50×10^4	5.48×10^7	1.22×10^5	1.95×10^8
1.65	6.81×10^4	7.85×10^7	1.25×10^5	2.48×10^8
1.8	8.63×10^4	1.09×10^8	1.31×10^5	2.80×10^8
2.0	1.09×10^5	1.54×10^8	1.35×10^5	3.02×10^8

Figure 1. Depiction of the generated flux for acoustic waves (solid) and longitudinal flux tube waves (dashed) as function of frequency for a mixing length of $\alpha_{\mathrm{ML}} = 1.8$. For the magnetic waves we consider the model with a bottom magnetic field strength of 1700 Gauss.

acoustic energy fluxes along with the wave frequency spectra; furthermore, they utilize an extended Kolmogorov spectrum with a modified Gaussian frequency factor. Both the acoustic and magnetic wave energy fluxes depend on the mixing-length parameter α_{ML}, for which $\alpha_{\mathrm{ML}} = 1.8$ is used (Stein et al., 2009a,b).

According to the updated value of α_{ML}, the initial wave energy flux for the acoustic model is given as $F_{\mathrm{M}} = 1.09 \times 10^8$ erg cm^{-2} s^{-1} (Ulmschneider et al., 1996); see Table 1. For the wave energy flux of the longitudinal flux tube wave we use $F_{\mathrm{M}} = 2.80 \times 10^8$ erg cm^{-2} s^{-1} (Fawzy & Cuntz, 2011); this value assumes a pressure ratio between outside and inside of the tube of $\epsilon = 3$ (see Eq. 5). It is based on the assumption of an inside magnetic field strength of 1700 G, noting that in our model the equipartition magnetic field strength is given as $B_{\mathrm{eq}} = \sqrt{8\pi p_e} = 2082$ G with $B/B_{\mathrm{eq}} \simeq 0.82$. The adopted inside tube magnetic field strength has been taken at an optical depth of $\tau_{5000} = 1.3$, corresponding to a mass column density of 2.1 g cm^{-2}. It is found that the longitudinal wave energy flux is increased relative to the acoustic energy flux by a factor of 2 to 3.5, depending on the mixing-length parameter α_{ML}, owing to decisive differences in the turbulent velocity v_t, which is considerably enhanced in the magnetic case (e.g., Ulmschneider & Musielak, 1998).

For previous elaborations on the appropriate value for F_{M} and B_{eq} see, e.g., Ulmschneider, Musielak & Fawzy (2001). Detailed studies of magnetic field strengths for solar flux tubes have been given by, e.g., Stenflo (1978)

and Solanki (1993), allowing us to motivate our choice of B_{eq}. Information on the wave frequency spectra for longitudinal flux tube waves was presented by, e.g., Ulmschneider & Musielak (1998) and Ulmschneider et al. (2001); see Fig. 1 for the spectral wave energy distribution serving as basis for our models[2]. These authors found that the spectral energy distribution for both the acoustic and longitudinal frequency spectrum has a maximum close to a wave period of 60 s. As our study also includes monochromatic waves, this value will be used in the following for both the acoustic and longitudinal wave study.

There is also considerable previous work on the most appropriate value for the initial wave energy flux of longitudinal tube waves; the latter is also modestly affected by the solar photospheric opacities owing to their influence on the construction of the solar tube models (i.e., attainment of radiative equilibrium, position of optical depth τ_{5000}). Previous work by Ulmschneider et al. (2001) adopted the opacity tables compiled by Bohn (1984) and Ulmschneider et al. (1996), whereas more recent simulations (Fawzy, 2010) use the opacity table given by R. L. Kurucz and collaborators (see Castelli & Kurucz 2004 for details).

This latter approach is adopted in the present paper. In principle, the opacity table by R. L. Kurucz and collaborators yields noticeably lower initial wave energy fluxes, which for α_{ML} between 1.8 and 2.0 are reduced by typically 30% compared to the models based on the opacity table considered by Ulmschneider et al. (2001). A relatively high initial wave energy flux based on $\alpha_{\mathrm{ML}} = 2.0$ was also adopted by Rammacher & Cuntz (2005a), which is a further reason for revisiting the propagation and dissipation of longitudinal tube waves in the Sun by considering an advanced treatment of the hydrodynamic and thermodynamic features as well as a realistic initial wave energy flux. Future investigations of stellar convection and photospheres may also be based on the massively parallel recently developed code Bifrost (Gudiksen et al., 2011), which is designed to simulate stellar atmospheres from the convection zone to the corona.

---

[2] The longitudinal wave energy spectrum as obtained through the study of nonlinear time-dependent responses of theoretical solar flux tubes to external pressure fluctuations (e.g., Ulmschneider & Musielak, 1998) is found to be somewhat bumpy, which is a consequence of the occurrence of large-amplitude perturbations (i.e., spiky waves) that are still apparent after temporal averaging has been applied.
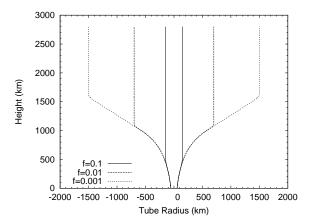
Figure 2. Spread of magnetic flux tubes for the different magnetic filling factors.
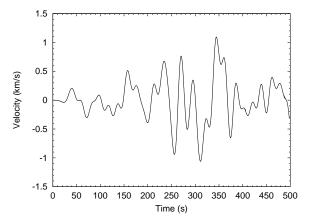

Figure 3. Velocity at the bottom boundary of the flux tube models in response to the longitudinal wave energy spectrum.

2.4 Flux tube models

For our models we consider three different flux tube geometries characterized by different amounts of spreading as function of height; see, e.g., Rammacher & Ulmschneider (1989) and Fawzy et al. (1998) for previous work on the effects of tube spreading on the deposition of non-radiative energy and the formation of chromospheric emission with focus on the Sun. The bottom radii of the tube models are chosen as 55 km corresponding to half of the photospheric pressure scale-height; note that the base pressure of the tubes is closely aligned to the VAL-C model (Vernazza et al., 1981). We also assume a magnetic field strength at the bottom of the tubes of $B_0 = 1700$ G informed by previous studies (Fawzy et al., 1998). We again consider wine-glass shaped tubes with top opening radii of 150 km, 700 km and 1500 km, respectively (see Table 2). For these tubes, exponential spreading is assumed at relatively low heights, followed by linear spreading. Full spreading is attained at heights of 571 km, 1126 km and 1639 km, respectively; see Fig. 2 for a depiction of the adopted tube models.

The tube with a top opening radius of 700 km has a top opening area approximately twenty times larger than the tube with 150 km. Moreover, the difference in the opening areas between the wine-glass tubes with opening radii

Table 2. Magnetic tube models.

f (%)	r_B (km)	r_T (km)	$B(r_\mathrm{T})$ (G)
0.1	55	150	229
0.01	55	700	10.5
0.001	55	1500	2.3

of 700 and 1500 km is a factor of 4.6. The flux tubes represent regions with magnetic filling factors $f = r_\mathrm{B}^2/r_\mathrm{T}^2$ equal to 0.1%, 0.01% and 0.001%, respectively, with r_B and r_T denoting the base radius and top radius of the tube, respectively. The effect of flux tube spreading results in a progressively lower inside magnetic field strength with a decreasing magnetic filling factor f, entailing $B(r_\mathrm{T}) = 2.3$ G for $f = 0.001$ compared to 229 G for $f = 0.1$ (see Table 2).

3 RESULTS AND DISCUSSION

3.1 Detailed time-dependent model simulations

By adopting the wave energy flux and wave frequency spectrum for $\alpha_\mathrm{ML} = 1.8$, we pursued detailed simulations for longitudinal tube waves for three different flux tubes (see Sect. 2.4); in the following, we show calculations pertaining to the magnetic filling factors of $f = 0.1\%$ and 0.001%. The stochstic velocity function at the bottom of the tubes owing to the application of the longitudinal wave frequency spectrum is depicted in Fig. 3. Time-dependent ionization has been considered for hydrogen as well as for Ca II and Mg II. To demonstrate the structure of our dynamic models in conjunction with the impact of different tube spreadings, we depict snapshots at identical elapsed times, which are: 400, 800, and 1400 s (see Fig. 4).

The general behaviour of the depicted waves in these models is characterized by temporal increases of the wave amplitudes resulting in the formation of shocks, typically occurring near 700 and 800 km for $f = 0.1\%$ and 0.001%, respectively. The tube geometry determines the general position of the chromospheric temperature rise. It is found that the larger the tube spreading, the greater the height of the temperature rise. In models of negligible tube spreading, the shock amplitudes tend to stay constant or increase as function of height. However, this behaviour is counteracted by the impact of tube spreading: the larger the spreading of the tube, the greater the area over which the wave energy is distributed (i.e., geometrical dilution), resulting in smaller wave amplitudes (see also Sect. 3.3).

Both models are shaped by strong interaction of shocks, which leads to increased shock strengths M_s as function of height. The shock strength M_s is given as

$$M_s = \frac{U_\mathrm{sh} - u_1}{c_\mathrm{T1}}, \tag{14}$$

where U_sh denotes the shock speed, and u_1 and c_T1 denote the gas speed and tube speed in front of the shock, respectively.

This behaviour is most pronounced for relatively narrow tubes; for example, we find that the main shock at $t = 1400$ s in the model of $f = 0.1\%$ has a strength of 6.62 compared to 1.02 in the model of $f = 0.001\%$. This type of behaviour is
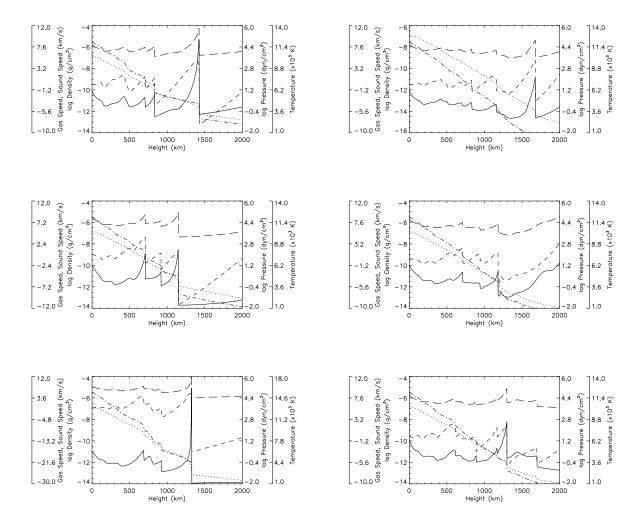
Figure 4. Two sequences of snapshots of longitudinal wave computations for magnetic flux tubes with filling factors of $f = 0.1\%$ (left column) and $f = 0.001\%$ (right column) based on time-dependent ionization and with consideration of frequency spectra. These filling factors correspond to tube opening radii of 150 km and 1500 km, respectively. We depict the following variables: temperature (solid lines), gas speed (dashed lines), density (short-dashed lines), sound speed (long-dashed lines), and gas pressure (dashed-dotted lines). The snapshots are taken at times of 400, 800, and 1400 s (top to bottom).

also mirrored by the jump in temperature across the shocks. The corresponding post-shock temperatures are typically considerably higher at relatively large atmospheric heights and in models of relatively narrow tubes, noting that narrow tubes imply higher shock strengths anyhow and, moreover, entail more intense shock merging. For $f = 0.1\%$ at an elapsed time of 1400 s (see Fig. 4), the attained post-shock temperatures range between 4650 and 16,170 K. In models of smaller magnetic filling factors, the post-shock temperatures are typically considerably lower; additionally, the variations in post-shock temperatures for given models simulations and time steps is also reduced. Furthermore, in models of time-dependent ionization, the post-shock temperatures are also considerably higher than in equivalent models without time-dependent ionization, a behaviour consistent with previous acoustic models (e.g., Carlsson & Stein, 1992, 1995; Rammacher & Ulmschneider, 2003); see also Sect. 3.2.

Additionally, the occurrence of stronger shocks in models of $f = 0.1\%$ compared to $f = 0.001\%$ results in higher

levels of momentum transfer, which typically lead to smaller densities in the top regions of those tubes as well as characteristic behaviours for the time-averaged temperatures (see Sect. 3.3). Although relatively large gas speeds may be attained by this process, the outflow speeds typically remain subsonic. Additionally, due to energy dissipation and radiative energy losses, the wave energy fluxes considerably decreases with atmospheric height (see Table 3 and 4). However, comparing tubes of $f = 0.1\%$ and 0.001%, the decrease in the wave energy flux with height regarding the tube with $f = 0.001\%$ is significantly less than expected from the degree of geometrical dilution. This phenomenon is caused by the relatively low density in the tube with $f = 0.1\%$ owing to the action of strong shocks (see Sect. 3.3); for previous results on adiabatic LTW simulations see, e.g., Fawzy et al. (1998). At a height of 2000 km, the wave energy fluxes are given as 5.10×10^3 and 1.93×10^3 ergs cm^{-2} s^{-1} for $f = 0.1\%$ and 0.001%, respectively (see Table 4). For the intermediate models of $f = 0.01\%$ (not shown), the wave energy
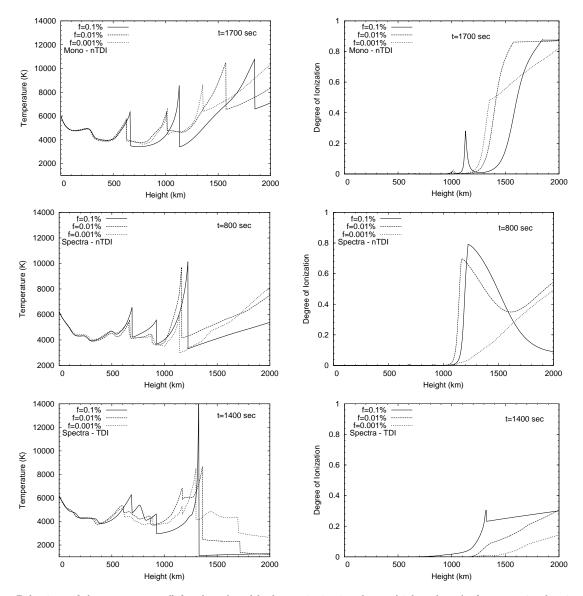
Figure 5. Behaviour of the temperature (left column) and hydrogen ionization degree (right column) of propagating longitudinal flux tube waves concerning tube models with different spreadings, which correspond to filling factors of $f = 0.1\%$, 0.01%, and 0.001%. We depict monochromatic wave models (top) and models with frequency spectra (middle) without time-dependent ionization as well as models with frequency spectra including time-dependent ionization (bottom). Note the vast differences in the temperature amplitudes. The very large temperature spike in the model with $f = 0.1\%$ (bottom) reaches 16,170 K.

flux at 2000 km is given as 4.17×10^3 ergs cm^{-2} s^{-1}. At low chromosphere heights, the heating and energy dissipation rates are identified as almost independent of the magnetic filling factor consistent with observational constraints (Bruls & Solanki, 1993).

3.2 Effects of flux tube spreading and time-dependent ionization

To obtain further insight into the effect of tube spreading on the atmospheric shock strengths as well as into other features owing to time-dependent ionization we computed a set of detailed models. They include monochromatic wave models without time-dependent ionization as well as models with frequency spectra with and without time-dependent ioniza-

tion. For each set of models, we considered tube spreadings corresponding to magnetic filling factors of $f = 0.1\%$, 0.01%, and 0.001%, respectively, thus allowing us to gauge the impact of tube spreading on the temperature structure and shock strengths.

The first set of models is based on monochromatic waves. For all three tube spreadings we chose an elapsed time of 2500 s, thus ensuring appropriate comparisons between the models. Hence, almost 30 shocks have been inserted into the atmosphere; therefore, all three tube atmospheres have reached a dynamic steady-state, i.e., the interaction between the shocks (i.e., ongoing shock merging) has subsided. Comparions between models of different tube spreading (see Fig. 5; top panel) indicate that the models with narrow tube spreading (i.e., high magnetic filling factor) are charac-

Table 3. LTW energy flux: monochromatic waves.[a]

Height	nTDI		TDI	
...	$f = 0.1$	$f = 0.001$	$f = 0.1$	$f = 0.001$
(km)	...	...	...	...
600	1.43×10^7	7.48×10^6	1.08×10^7	1.56×10^6
900	2.21×10^6	4.15×10^5	1.97×10^6	1.01×10^5
1200	2.62×10^5	1.01×10^4	2.56×10^5	2.79×10^3
2000	1.02×10^4	3.37×10^3	4.87×10^3	2.67×10^2

[a] The LTW energy fluxes are given in ergs cm^{-2} s^{-1}.

Table 4. LTW energy flux: spectral waves.[a]

Height	nTDI		TDI	
...	$f = 0.1$	$f = 0.001$	$f = 0.1$	$f = 0.001$
(km)	...	...	...	...
600	1.09×10^7	3.24×10^6	1.53×10^7	3.49×10^6
900	2.75×10^6	4.90×10^5	3.33×10^6	5.49×10^5
1200	4.30×10^5	3.31×10^4	5.07×10^5	2.58×10^4
2000	4.34×10^4	5.41×10^3	5.10×10^3	1.93×10^3

[a] The LTW energy fluxes are given in ergs cm^{-2} s^{-1}.

terized by relatively high shock strengths, whereas models with wide tube spreading (i.e., low magnetic filling factor) are shaped by relatively small shock strengths. Specifically, for regions beyond 1200 km, the typical shock strength for $f = 0.1\%$ varies between $M_s = 1.85$ and 2.77, whereas for $f = 0.001\%$, it is only $M_s = 1.60$. For $f = 0.01\%$, intermediate shock strength values are found, as expected. In models of monochromatic waves the shocks have attained limiting shock strength, which is found to depend on the height-dependent behaviour of the tube spreading, as previously pointed out through analytical means (Cuntz, 2004). Previous simulations for solar flux tubes based on adiabatic LTW waves without time-dependent ionization also show a similar kind of behaviour (Fawzy et al., 1998). Due to the omission of detailed time-dependent ionization, it is found that the degree of hydrogen ionization at 2000 km is about 95% for $f = 0.1\%$ and 0.01%. For $f = 0.001\%$, a lower value for the hydrogen ionization degree is found; in this case, a smooth and steady increase of the hydrogen ionization degree occurs between 1200 and 2000 km.

The second and third sets of models are based on LTW frequency spectra. Figure 5 (middle and bottom panel) shows snapshots without and with the consideration of time-dependent ionization, respectively. For both types of models, we again consider magnetic filling factors of $f = 0.1\%$, 0.01%, and 0.001%. The snapshots displayed for these sets of models are taken at 800 and 1400 s, respectively; furthermore, the elapsed time of simulation is about 2000 s. The main shocks in Fig. 5 (middle panel), attained through the process of shock merging, have strengths of 3.19, 3.18, and 2.11, respectively. The main shock for $f = 0.1\%$ has a post-shock temperature of 10,070 K; the hydrogen ionization degree in front of the shock is 78%, and shortly behind the shock it is close to zero. By comparison, the post-shock temperatures of the main shocks pertaining to $f = 0.01\%$ and 0.001% are 9250 K and 6470 K, respectively, which clearly

indicates the impact of tube spreading. Clearly, the change of structure due to different magnetic filling factors is a direct consequence of the dilution of the wave energy flux (see Table 4), including associated magnetohydrodynamic, thermodynamic and radiative phenomena, particularly those associated with the formation of shocks of different strengths. At heights of 1200 km, the wave energy flux is reduced by factors of 1.5×10^{-3}, 2.9×10^{-4}, and 1.9×10^{-5} in tube models with $f = 0.1\%$, 0.01%, and 0.001%, respectively.

Figure 5 (bottom panel) reflects a similar setting but now both time-dependent ionization and LTW frequency spectra are taken into account. The main difference to the kind of simulations previously discussed is an enhanced tendency of building up very strong shocks due to shock merging, particularly for the model with a magnetic filling factor of 0.1%. In this case, a very large temperature spike with a post-shock temperature of 16,170 K is found to occur; the corresponding shock strength is given as $M_s = 6.62$. In contract, however, at relatively low heights, a considerable number of small shocks is encountered. Moreover, at heights between 600 and 1000 km, shock strengths are typically between $M_s = 1.2$ and 1.5 in models of $f = 0.1\%$. The shock strengths are even lower in models with 0.001%; in the latter cases, the shock formation is postponed to larger heights. The merging of shocks leads to the build-up of very strong shocks, a process that is significantly amplified in models of time-dependent ionization, owing to the fact that virtually no energy is used immediatelly behind the shocks to ionize hydrogen (or any other species). Therefore, an increased amount of energy is available to further increase the post-shock temperatures.

The dilution of the wave energy flux is also highly significant in these types of models depending on the degree of geometrical spreading. At heights of 1200 km, the initial wave energy flux is reduced by factors of 1.8×10^{-3}, 3.9×10^{-4}, and 9.2×10^{-5}, in models with $f = 0.1\%$, 0.01%,
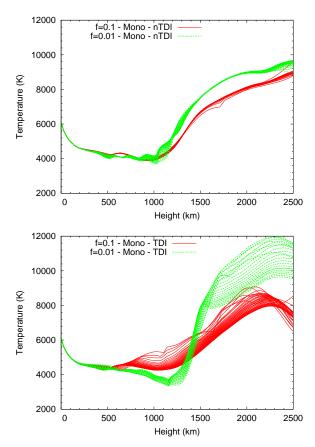
Figure 6. Build-up of mean (i.e., time-averaged) temperatures for models with and without time-dependent ionization (bottom and top figure, respectively). Note the influence of the different tube spreadings, denoted as magnetic filling factors $f = 0.1\%$ and 0.01%; see Table 2. The time of averaging for the various models is close to 60 s. For the simulations with time-dependent ionization the averaging starts at 513 s ($f = 0.1\%$) and 821 s ($f = 0.01\%$) and for the simulations without time-dependent ionization it starts at 607 s ($f = 0.1\%$) and 612 s ($f = 0.01\%$).

and 0.001%, respectively. However, an assessment of the absolute amount of wave energy flux indicates (see Table 3 and 4) that it is less diluted than expected from the degree of geometrical dilution, which obviously is a factor of 100 between $f = 0.1\%$ and 0.001%. The reason for this type of behaviour is that models with $f = 0.1\%$ have a lower overall density; furthermore, in those models there is a higher loss of energy behind the shocks due to enhanced radiative energy losses and the initiation of episodic outflow. For the same reason, the reduction of the wave energy flux with height is also more drastic in models with time-dependent ionization compared to models without consideration of this process (TDI versus nTDI).

For the assortments of small shocks, it is noteworthy that different shock strengths correspond to different shock speeds; therefore, the shocks in models with LTW frequency spectra are poised to overtake one another, thus invoking significant shock merging as well as the build up of very strong shocks. This result has already been obtained in 1-D acoustic models (e.g., Cuntz, 1987), and it is evident in 1-D LTW models with and without the consideration of time-dependent ionization, but it is drastically enhanced if

time-dependent ionization of hydrogen is considered. The occurrence of very strong shocks is a typical feature of the combined influence of frequency spectra and time-dependent ionization inherent in 1-D (magneto-) hydrodynamic models; see, e.g., Carlsson & Stein (1992) for previous results on acoustic models. Figure 5 (middle and bottom panels) also depicts the behaviour of the hydrogen ionization degree in the various models in front and behind the shocks. Clearly, the hydrogen ionization degrees are progressively lower in models of smaller values of f; however, in models without time-dependent ionization of hydrogen it drops to almost zero in the post-shock regions (see Fig. 5, middle panel), whereas in models with time-dependent ionization of hydrogen it is essentially maintained (see Fig. 5, bottom panel).

3.3 Behaviour of time-averaged temperatures and ionization degrees

Additional insight into the overall dynamic structure of flux tubes subjected to the propagation and dissipation of longitudinal tube waves can be obtained by assessing the behaviour of time-averaged temperatures. Again, we considered both monochromatic and spectral waves, while pursuing detailed comparisons for models with and without time-dependent ionization. Concerning monochromatic models, we also pursued computations for acoustic waves aimed at representing atmospheric structure exterior to the flux tubes; in this regard, plane-parallel geometry was assumed. In all types of models, the wave energy generation was derived from a mixing length of $\alpha_{ML} = 1.8$ resulting in an initial wave energy flux of 1.09×10^8 and 2.80×10^8 erg cm^{-2} s^{-1} for the acoustic and magnetic models, respectively (see Table 1). For the magnetic flux tube simulations, we again considered tube geometry given by magnetic filling factors of $f = 0.1\%$, 0.01%, and 0.001%. Examples for the steady build-up of time-averaged temperatures owing to the implemented averaging procedure are conveyed in Fig. 6.

Detailed information on the behaviour of the time-averaged temperatures is given in Fig. 7, which depicts a total of 14 models. Let us first focus on the evaluation of dynamic magnetic flux tube models based on monochromatic waves. Typically, we awaited the insertion of 20 to 50 wave periods into the atmosphere prior to the evaluation of mean (i.e., time-averaged) quantities to ensure that the switch-on behaviour of the tube atmospheres has subsided and dynamic equilibria have been reached. The time-averaged temperatures of the various tube models as well as those of the acoustically heated models are relatively similar at heights below 800 km, although they are found to be highest in the model with the smallest spreading (i.e., $f = 0.1\%$), as expected. This latter result can be understood based on the dilution of the wave energy flux, which also affects the height of shock formation. The latter is given as 400, 550, and 850 km for the models with 0.1%, 0.01%, and 0.001%, respectively. For the acoustic model, the height of shock formation is given as 600 km. Only minor differences are obtained between models with and without time-dependent ionization, noting that due to the relatively high densities, low temperatures and small shock strengths (if any), the effects due to time-dependent ionization are less pronounced.

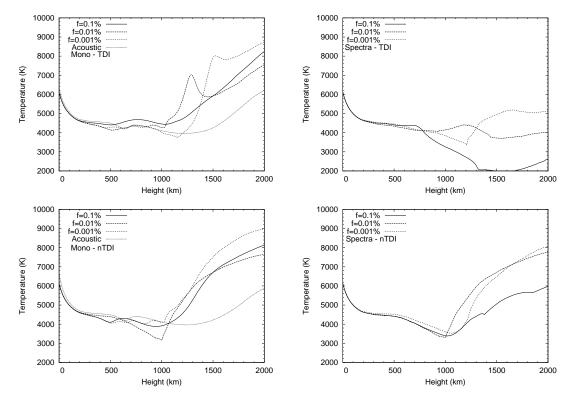In the upper parts of the tube atmospheres, the tem-

Figure 7. Comparison of time-averaged temperatures for longitudinal wave computations pertaining to different types of models. We show models based on monochromatic waves (left column) and frequency spectra (right column). The top and bottom row depicts models with and without consideration of time-dependent ionization, respectively. Concerning the model series based on monochromatic waves, we also show acoustic wave models for comparison. Regarding the magnetic flux tubes models, we show simulations for magnetic filling factors of $f = 0.1\%$, 0.01%, and 0.001%.

peratures in the model of the widest tube opening radius are expected to be lowest due to the largest dilution of the wave energy flux. The difference in dilution is expected to be a factor of 100 between $f = 0.1\%$ and 0.001%; however, it is significantly lower, i.e., a factor between 3 and 26 for models with or without time-dependent ionization and with or without the consideration of LTW frequency spectra (see Table 3 and 4). For some portions of the tube atmospheres, it is even found that "the larger the tube opening radius, the higher the mean temperatures", a result that is highly counter-intuitive. The reason for this behaviour is that the dilution of the wave energy flux does not exactly follow geometrical scaling. Other relevant processes involve the density structure within the flux tubes as well as significant dynamical and radiative processes, especially pertaining to strong shocks, including significant radiative energy losses. Comparing models with and without time-dependent ionization reveals that time-dependent ionization leads to lower average temperatures inside the flux tubes compared to time-independent ionization. However, the average temperatures inside of flux tubes in models with or without time-dependent ionization are nonetheless noticeably higher than in the acoustically heated external atmosphere, pointing to the significance of magnetic heating.

We also pursued corresponding sets of models based on LTW frequency spectra instead of monochromatic waves. In this type of models the attained time-averaged temperatures were unrealistically low, particularly in models of time-dependent ionization. In this case, the combined effects

of time-dependent hydrogen ionization and of the dynamical structure related to the propagation of spectral waves lead to very strong shocks, which invoked amplified energy losses behind the shocks as well as strong atmospheric expansions associated with quasi-adiabatic cooling; see, e.g., Gail, Cuntz & Ulmschneider (1990) and Koninx & Pijpers (1992) for theoretical work on the build-up of wave pressure due to shocks. The impact of very strong shocks entailed that the time-averaged temperatures are lowest in models with small tube spreading, i.e., high magnetic filling factors (e.g., case of $f = 0.1\%$) if time-dependent ionization of hydrogen is taken into account.

Finally, we studied the behaviour of the height-dependent time-averaged hydrogen ionization in our set of models (see Figs. 8 and 9). We found that the hydrogen ionization degrees steadily increase at heights beyond 1200 km regardless of the magnetic filling factor, i.e., the tube top opening radius. However, in general, they remain relatively low (i.e., below 40%) in models with time-dependent ionization (TDI), whereas they are found to be relatively high (i.e., between 70% and 90% at heights beyond 2000 km) in models without time-dependent ionization (nTDI). This is consistent with the general behaviour of time-dependent hydrogen ionization as described, as in this case lower degrees of ionization occur at most heights, including regions behind shocks, including strong shocks owing to the time-delay of ionization in accord to the time-dependent statistical rate equations (see Sect. 2.1).

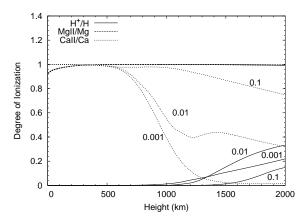We also evaluated time-dependent effects for the ion-

Figure 8. Comparison of the time-averaged ionization degrees for hydrogen, magnesium and calcium concerning longitudinal wave computations with time-dependent ionization and with consideration of frequency spectra. We depict results for magnetic flux tubes with filling factors of $f = 0.1\%$, 0.01%, and 0.001%.
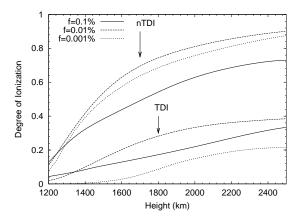

Figure 9. Comparison of time-averaged hydrogen ionization degrees for longitudinal wave computations with (TDI) and without (nTDI) time-dependent ionization regarding models based on frequency spectra. We depict results for magnetic flux tubes with filling factors of $f = 0.1\%$, 0.01%, and 0.001%.

ization of calcium and magnesium (see Fig. 8), noting that Ca II and Mg II are of significant importance for the facilitation of radiative cooling (see Sect. 2.2). Our simulations show that most of the magnesium is ionized to Mg II at most heights regardless of the geometrical filling factor of the respective flux tube. However, for Ca II the height-dependent behaviour of the ionization degree is strongly impacted by the geometrical spread of the flux tubes (see Fig. 2). Generally, for smaller values of f, associated with a lesser dilution of the wave energy flux, a larger fraction of calcium is ionized to Ca II. The appropriate explanation is the lower dilution of the wave energy flux in those models, leading to more effective shock heating and higher overall temperatures.

4 SUMMARY AND CONCLUSIONS

We pursued sets of time-dependent model simulations for solar magnetic flux tubes with focus on longitudinal tube waves with and without the consideration of time-dependent

ionization, particularly pertaining to hydrogen. The treatment of longitudinal tube waves is motivated by a large variety of studies including work by Hasan & van Ballegooijen (2008) arguing that longitudinal tube waves are able to provide quasi-steady heating sufficient to explain the bright solar network grains observed in Ca II H and K. We studied the dynamics of flux tubes with different magnetic filling factors, i.e., 0.1%, 0.01%, and 0.001%, corresponding to different tube top opening radii, guided and motivated by previous observational results (e.g., Spruit & Roberts, 1983; Solanki, 1996). It was found that the dynamic tube structures are determined by a complex interplay between shock heating, radiative and hydrodynamic cooling (with the latter caused by wave pressure), dilution of the wave energy flux due to the flux tube geometry, and time-dependent ionization. We identified pronounced differences between the tubes models especially in regard to tubes with different tube opening radii and in response to the inclusion or omission of time-dependent ionization.

Similar to the case of acoustic waves, time-dependent ionization in LTW models leads to a large range of phenomena, such as over- and underionization of the flow, increased temperature jumps at shocks, and modified mean (i.e., time-averaged) temperature, density and ionization structures. The impact of time-dependent treatment of ionization for flux tubes becomes evident through comparisons of mean temperatures between the different types of models. Regarding monochromatic models it was found that time-dependent ionization leads to lower average temperatures inside flux tubes compared to time-independent ionization, an effect already known for acoustically heated models.

However, the average temperatures inside of flux tubes in models with and without time-dependent ionization are nonetheless noticeably higher than in the acoustically heated external atmosphere. If monochromatic longitudinal tube waves are used, the mean (i.e., time-averaged) temperatures of the tubes generally show a quasi-steady increase with height. However, if frequency spectra are used, the mean temperatures, in essence, show no rise with height at all. This behaviour is initiated by the formation of very strong shocks (especially in narrow tubes, corresponding to small magnetic filling factors) resulting in large-scale quasi-adiabatic cooling, leading to unrealistically low temperatures. This type of result has already previously been found in corresponding 1-D models of acoustic waves (e.g., Carlsson & Stein, 1992, 1995; Rammacher & Ulmschneider, 2003), a behaviour deemed highly unrealistic (Ulmschneider et al., 2005).

An appropriate enhancement of our current models will be the calculation of self-consistent 3-D magnetohydrodynamic (MHD) models. Those models face, however, the principal challenge of the necessity to include both detailed multi-level 3-D radiative transfer and 3-D flows including the detailed treatment of shock formation and shock interaction. Important progress has already been made (e.g., Stein et al., 2009a,b), but further efforts are needed to obtain of a concise picture. Tentative insights into the principal properties of these types of future models can be attained through inspecting existing 3-D time-dependent *non-magnetic* hydrodynamics models, which also consider time-dependent non-equilibrium effects caused by hydrogen (Leenaarts & Wedemeyer-Böhm, 2006), albeit various

restrictive assumptions including (but not limited to) the lack of back-coupling of the ionization to the equation of state. In this type of models it is found that the build-up of strong shocks due to shock interaction is largely absent, resulting in a lack of unrealistically high cooling behind the strong shocks previously also referred to as "hydrodynamic refrigeration" (Cuntz & Muchmore, 1994). In this case a quasi-steady rise of temperature with height is attained, which appears to be in close resemblance to empirical solar chromosphere models (e.g., Anderson & Athay, 1989). Nonetheless, our results based on time-dependent ionization and LTW frequency spectra allow insight into the limiting case of 1-D geometry, while also noting that our models based on time-dependent ionization and monochromatic waves are expected to be approximately reflective of physical reality.

An alternative, or perhaps supplementary, way of supplying chromospheric heating might be given through ambipolar diffusion as described by Khomenko & Collados (2012). Here the presence of neutrals, together with the decrease with height of the collisional coupling, leads to deviations from the classical magnetohydrodynamic behaviour of the chromospheric plasma. Khomenko & Collados (2012) pointed out that a relative net motion occurs between the neutral and ionized components, referred to as ambipolar diffusion. According to this model, the dissipation of currents in the chromosphere is enhanced by orders of magnitude due to the action of ambipolar diffusion, as compared with the standard ohmic diffusion. The authors proposed that a significant amount of magnetic energy can be released to the chromosphere just by existing force-free 10–40 G magnetic fields there.

Additional studies were given by Fedun, Erdélyi & Shelyag (2009), Vigeesh, Hasan & Steiner (2009), and Erdélyi & Fedun (2010). Fedun et al. (2009) studied the oscillatory response of the 3-D solar photosphere to the leakage of photospheric motion. They found, among other results, that high-frequency waves propagate from the lower atmosphere across the transition region experiencing relatively low reflection, and transmitting most of their energy into the corona, and, furthermore, that the magnetic field acts as a waveguide for both high- and low-frequency waves originating from the photosphere and propagating up into the solar corona. Vigeesh et al. (2009) provided a targeted study on wave propagation and energy transport in the magnetic network of the Sun based on 2-D MHD simulations, which among other results identified the limited capacity of acoustic waves. Erdélyi & Fedun (2010) investigated the oscillatory modes of a magnetically twisted compressible flux tube embedded in a compressible magnetic setting, including applications to solar magneto-seismology.

As an overarching statement concerning our study we conclude that the significance of time-dependent ionization identified in the simulations of longitudinal tube waves is a stark motivation to also consider this type of effect in future models of transverse and torsional tube waves. This will allow to obtain a more detailed picture of the dynamics and energetics of solar-type outer atmospheres. This obvious suggestion is also supported by the repeatedly obtained finding that longitudinal flux tube waves, as gauged through models considering time-dependent ionization phenomena as

done in the present study, are insufficent to supply an adequate amount of energy for balancing coronal heating in the view of early and updated estimates by Güdel (2007) and others.

References

Anderson L. S., Athay R. G., 1989, ApJ, 346, 1010
Avrett E. H., 1985, in Lites B. W., ed., Chromospheric Diagnostics and Modeling. NSO, Sacramento Peak, p. 67
Beck C. A. R., Rammacher W., 2010, A&A, 510, A66
Beck C. A. R., Rezaei R., Puschmann K. G., 2012, A&A, in press (arXiv:1206.1759)
Bello González N., Flores Soriano M., Kneer F., Okunev O., 2009, A&A, 508, 941
Bogdan T. J., et al., 2003, ApJ, 599, 626
Bohn H. U., 1984, A&A, 136, 338
Bruls J. H. M. J., Solanki S. K., 1993, A&A, 273, 293
Carlsson M., Stein R. F., 1992, ApJ, 397, L59
Carlsson M., Stein R. F., 1995, ApJ, 440, L29
Carlsson M., Stein R. F., 2002, ApJ, 572, 626
Castelli F., Kurucz R. L., 2004, in Piskunov N. E., Weiss W. W., Gray D. F., eds, ASP Conf. Ser., IAU Symp. 210, Stars as Suns: Modelling of Stellar Atmospheres. Astron. Soc. Pac., San Francisco, CD-ROM, Poster 20 (arXiv:astro-ph/0405087)
Cuntz M., 1987, A&A, 188, L5
Cuntz M., 2004, A&A, 420, 699
Cuntz M., Muchmore D. O., 1994, ApJ, 433, 303
Cuntz M., Suess S. T., 2004, A&A, 424, 1003
Cuntz M., Ulmschneider P., 1988, A&A, 193, 119
Cuntz M., Rammacher W., Ulmschneider P., Musielak Z. E., Saar S. H., 1999, ApJ, 522, 1053
Cuntz M., Rammacher W., Musielak Z. E., 2007, ApJ, 657, L57
Erdélyi R., Ballai I., 2007, AN, 328, 726
Erdélyi R., Fedun V., 2010, Sol. Phys., 263, 63
Fawzy D. E., 2010, MNRAS, 408, 293
Fawzy D. E., Cuntz M., 2011, A&A, 526, A91
Fawzy D. E., Ulmschneider P., Cuntz M., 1998, A&A, 336, 1029
Fawzy D. E., Rammacher W., Ulmschneider P., Musielak Z. E., Stępień K., 2002, A&A, 386, 971
Fedun V., Erdélyi R., Shelyag S., 2009, Sol. Phys., 258, 219
Fossum A., Carlsson M., 2005, Nature, 435, 919
Gail H.-P., Cuntz M., Ulmschneider P., 1990, A&A, 234, 359
Güdel M., 2007, Living Rev. Sol. Phys., 4, 3
Gudiksen B. V., Carlsson M., Hansteen V. H., Hayek W., Leenaarts J., & Martínez-Sykora J., 2011, A&A, 531, A154

Hasan S. S., van Ballegooijen A. A., 2008, ApJ, 680, 1542

Herbold G., Ulmschneider P., Spruit H. C., Rosner R., 1985, A&A, 145, 157

Kalkofen W., 2007, ApJ, 671, 2154

Khomenko E., Collados M., 2012, ApJ, 747, 87

Klimchuk J. A., 2006, Sol. Phys., 234, 41

Koninx J.-P. M., Pijpers F. P., 1992, A&A, 265, 183

Leenaarts J., & Wedemeyer-Böhm S., 2006, A&A, 460, 301

Lighthill M. J., 1978, Waves in Fluids. Cambridge Univ. Press, Cambridge

Linsky J. L., 1991, in Ulmschneider P., Priest E. R., Rosner R., eds, Mechanisms of Chromospheric and Coronal Heating. Springer, Berlin, p. 166

Mihalas D., Mihalas B. W., 1984, Foundations of Radiation Hydrodynamics. Oxford Univ. Press, New York

Musielak Z. E., 2004, in Dupree A. K., Benz A. O., eds, ASP Conf. Ser., IAU Symp. 219, Stars as Suns: Activity, Evolution and Planets. Astron. Soc. Pac., San Francisco, p. 437

Musielak Z. E., Rosner R., Stein R. F., Ulmschneider P., 1994, ApJ, 423, 474

Narain U., Ulmschneider P., 1996, Space Sci. Rev., 75, 453

Nieuwenhuijzen H., de Jager C., Cuntz M., Lobel A., Achmad L., 1993, A&A, 280, 195; Erratum 1999, 343, 661

Ofman L., Nakariakov V. M., DeForest C. E., 1999, ApJ, 514, 441

Ofman L., Nakariakov V. M., Sehgal N., 2000, ApJ, 533, 1071

Rammacher W., Cuntz M., 2003, ApJ, 594, L51

Rammacher W., Cuntz M., 2005a, in Favata F., Hussain G. A. J., Battrick B., eds, Cool Stars, Stellar Systems, and the Sun 13. ESA SP-560, Vol. II, p. 891

Rammacher W., Cuntz M., 2005b, A&A, 438, 721

Rammacher W., Ulmschneider P., 2003, ApJ, 589, 988

Rammacher W., Fawzy D. E., Ulmschneider P., Musielak Z. E., 2005, ApJ, 631, 1113

Rammacher W., Ulmschneider P., 1989, in Rutten R. J., Severino G., eds, Solar and Stellar Granulation. Kluwer, Dordrecht, p. 589

Roberts B., 2004, in Lacoste H., ed., SOHO 13: Waves, Oscillations and Small-Scale Transient Events in the Solar Atmosphere: A Joint View of SOHO and TRACE. ESA SP-547, p. 1

Schmitz F., Ulmschneider P., Kalkofen W., 1985, A&A, 148, 217

Schrijver C. J., 2001, ApJ, 547, 475

Schrijver C. J., Zwaan C., 2000, Solar and Stellar Magnetic Activity. Cambridge Univ. Press, Cambridge

Solanki S. K., 1993, Space Sci. Rev., 63, 1

Solanki S. K., 1996, in Strassmeier K. G., Linsky J. L., eds, IAU Symp. 176, Stellar Surface Structure. Kluwer, Dordrecht, p. 201

Solanki S. K., Roberts B., 1992, MNRAS, 256, 13

Spruit H. C., Roberts B., 1983, Nature, 304, 401

Steffen M., 1993, Habilitation Thesis, Univ. Kiel, Germany

Stein R. F., Nordlund Å., Georgobiani D., Benson D., Schaffenberger W., 2009a, in Dikpati M., Arentoft T., González Hernández I., Lindsey C., Hill F., eds, ASP Conf. Ser. Vol. 416, Solar–Stellar Dynamos as Revealed by Helio- and Asteroseismology. Astron. Soc. Pac., San Francisco, p. 421

Stein R. F., Georgobiani D., Schaffenberger W., Nordlund Å., Benson D., 2009b, in Stempels E., ed., AIP Conf. Proc. Vol. 1094, Cool Stars, Stellar Systems, and the Sun 15. AIP, Melville, p. 764

Stenflo J. O., 1978, Rep. Progr. Phys., 41, 865

Trampedach R., Christensen-Dalsgaard J., Nordlund Å., Stein R. F., 1997, in Pijpers F. P., Christensen-Dalsgaard J., Rosenthal C. S., eds, Solar Convection and Oscillations and their Relationship. Kluwer, Dordrecht, p. 73

Ulmschneider P., Musielak Z. E., 1998, A&A, 338, 311

Ulmschneider P., Musielak Z., 2004, in Pevtsov A. A., Uitenbroek H., eds, ASP Conf. Ser. Vol. 286, Current Theoretical Models and Future High Resolution Solar Observations: Preparing for ATST. Astron. Soc. Pac., San Francisco, p. 363

Ulmschneider P., Kalkofen W., Nowak T., Bohn U., 1977, A&A, 54, 61

Ulmschneider P., Theurer J., Musielak Z. E., 1996, A&A, 315, 212

Ulmschneider P., Musielak Z. E., Fawzy D. E., 2001, A&A, 374, 662

Ulmschneider P., Rammacher W., Musielak Z. E., Kalkofen W., 2005, ApJ, 631, L155

Vernazza J. E., Avrett E. H., Loeser R., 1981, ApJS, 45, 635

Vigeesh G., Hasan S. S., Steiner O., 2009, A&A, 508, 951

Wedemeyer-Böhm S., Scullion E., Steiner O., van der Voort L. R., de la Cruz Rodriguez J., Fedun V., Erdélyi R., 2012, Nature, 486, 505

Worrall G., 2012, Sol. Phys., 279, 43